BOUNDARY CONDITIONS FOR A FUSION PLASMA

R. Behrisch

BOUNDARY CONDITIONS FOR A FUSION PLASMA

R. BEHRISCH

Max-Planck-Institut für Plasmaphysik, EURATOM Association,
D-8046 Garching/München, Germany

Résumé. — Les conditions aux limites des plasmas actuels et des futurs plasmas de fusion sont déterminées par les interactions entre le plasma et la première paroi solide. La désorption provoquée par le contact entre plasma et paroi, domine actuellement, mais les phénomènes de rétrodiffusion d'ions, de trapping et réémission aussi bien que de pulvérisation sont dominants en présence de parois propres. Les flux vers la paroi sont indiqués pour plusieurs machines à plasma et les données concernant les processus élémentaires au niveau de la paroi sont passés brièvement en revue.

Abstract. — The boundary conditions in today's plasma experiments and in later fusion plasmas are determined by the interactions of the plasma with the first solid wall. In today's experiments desorption by the plasma hitting the wall dominates, but ion backscattering, trapping and release, as well as sputtering of wall material, will dominate in machines with cleaner walls. The fluxes to the first wall for some of today's plasma experiments are reported and the data about the elementary processes at the first wall are shortly reviewed.

1. **Introduction.** — An understanding and control of the plasma-wall interaction processes is, besides the question of MHD stability, transport properties and heating of plasmas, an important condition for achieving better plasma parameters in todays experiments aiming at a fusion reactor, especially of the tokamak type. Plasma wall interaction influences the plasma predominantly in two ways :

1) The magnetic confinement of the plasma is only poor and all plasma particles are lost to the first wall and recycled to the plasma several times during one discharge [1]. This means that the plasma parameters are determined by reflection, trapping and reemission, and by desorption of the plasma particles at the first wall.

2) The bombardment of the first wall by the plasma particles as well as the electromagnetic radiation causes a release of wall atoms, i.e. atoms with $z \geqslant 2$, which contaminate the plasma and considerably influence the properties of the plasma and by this the achievable plasma parameters [1] to [5]. In a future fusion reactor the release of wall atoms as well as the changes at the first wall due to the implantation of gas atoms pose the additional problems of wall erosion and degredation [6] to [14].

The recycling flux (point 1) is about 100 times larger than the impurity-, i.e. wall atom flux (point 2), but both are equally important. In computer simulations of a plasma they represent the boundary conditions for the solution of the differential equations describing the plasma behaviour [15].

In today's plasma experiments the details of the plasma wall interaction processes are not yet clear. Investigations have just been started [2] to [5]. On the other hand also the knowledge of the atomic data of the different interaction processes at the first wall is only poor [16] to [18]. In the following it is tried to summarise what is known in these areas and to outline some conclusions from the results.

2. **The plasma boundary and the fluxes to the first wall.** — In today's plasma experiments the plasma boundary is defined by a material limiter, mostly of Mo or W, in some cases by the separatrix of a magnetic divertor. This is shown schematically in figure 1. In the magnetic field for confining the plasma the particles move predominantly along the magnetic field lines on the magnetic surfaces. The diffusion perpendicular to the magnetic surfaces is much smaller, but still considerable, so that plasma particles continuously leak out at the plasma boundary. In further moving along the field lines these particles hit the sides of the limiter or are guided into the divertor chamber. Thus the sides of the limiter play a similar role as the divertor plates in catching those charged particles which have left the plasma boundary. Some results of measured plasma fluxes in the shadow of a limiter from recent experimental investigations [19, 20] are shown in figure 2*a-c*. The energy flux, the hydrogen flux, and the flux of impurities (Mo) were measured with a probe and show a decrease with increasing distance of the probe from the plasma boundary defined by a limiter. In each case some flux still reaches the first wall. We may assume that the

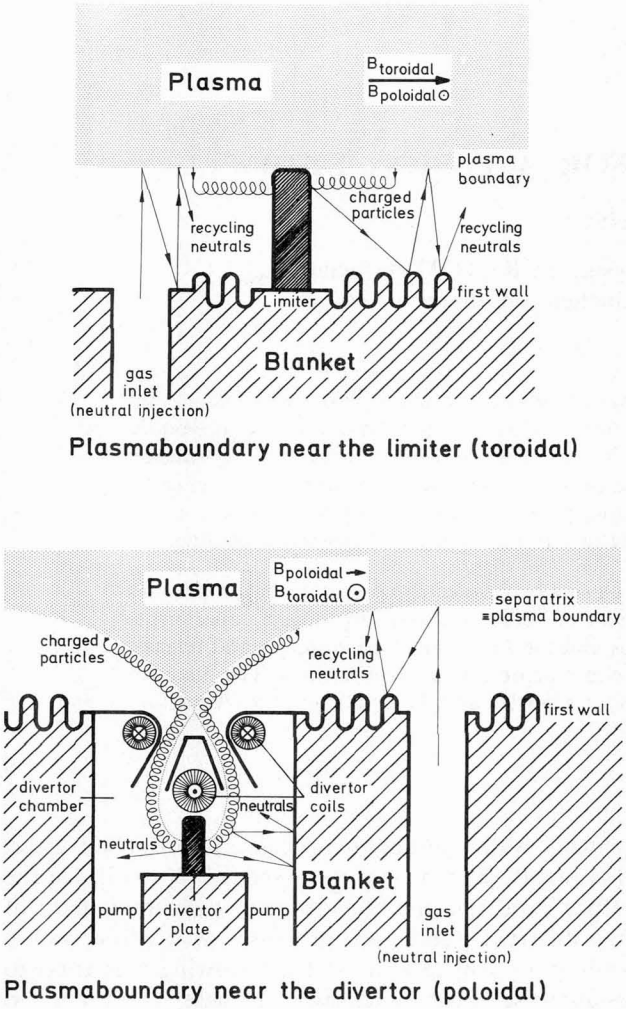

FIG. 1. — Schematic of the space between the plasma boundary and the first wall for the case of a limiter and no divertor and the case of a poloidal divertor.

flux close to the plasma boundary consists of charged particles which hit the probe. The hydrogen flux at the first wall consists predominantly of neutrals [19] created by charge exchange. The charge state of the impurities hitting the first wall is not yet known, but they may partly be neutrals as well.

An interpretation of the measured fluxes is difficult. The higher flux measured more close to the plasma may be just caused by the better confinement on a magnetic surface and thus a better collection efficiency on the probe. The total flux at the first wall, i.e. the measured flux density multiplied by the first wall area may be of the same order of magnitude or larger than the flux density measured closer to the plasma multiplied by the corresponding area of the sides of the limiter.

The energies of the particle fluxes have been determined only for the neutral hydrogen flux at the first wall using neutral particle detectors, which are sensitive only for energies above 200 eV. The measured energy distribution corresponds to the plasma temperature [21] with an increased flux at energies of the order of 100 eV [22]. As impurities thermalise very fast in the plasma, one may assume that they hit the limiter and first wall with the same energy as the hydrogen, but no measurements have been performed. At the beginning and the end of the discharge an increased flux has been observed in some cases [19, 23].

The intensities of the currents to the first wall have been measured, with large uncertainties in some cases, to be of the order of 10^{15} to 10^{16} hydrogen atoms/cm^2 s ($\sim$ 1 mA) [19] and 10^{11} to 10^{13} impurity atoms/cm^2 s ($\sim$ 1 μA) [24] in todays largest tokamaks. These intensities, the energies and the distributions of the fluxes depend largely on the discharge conditions, but this has not yet been investigated.

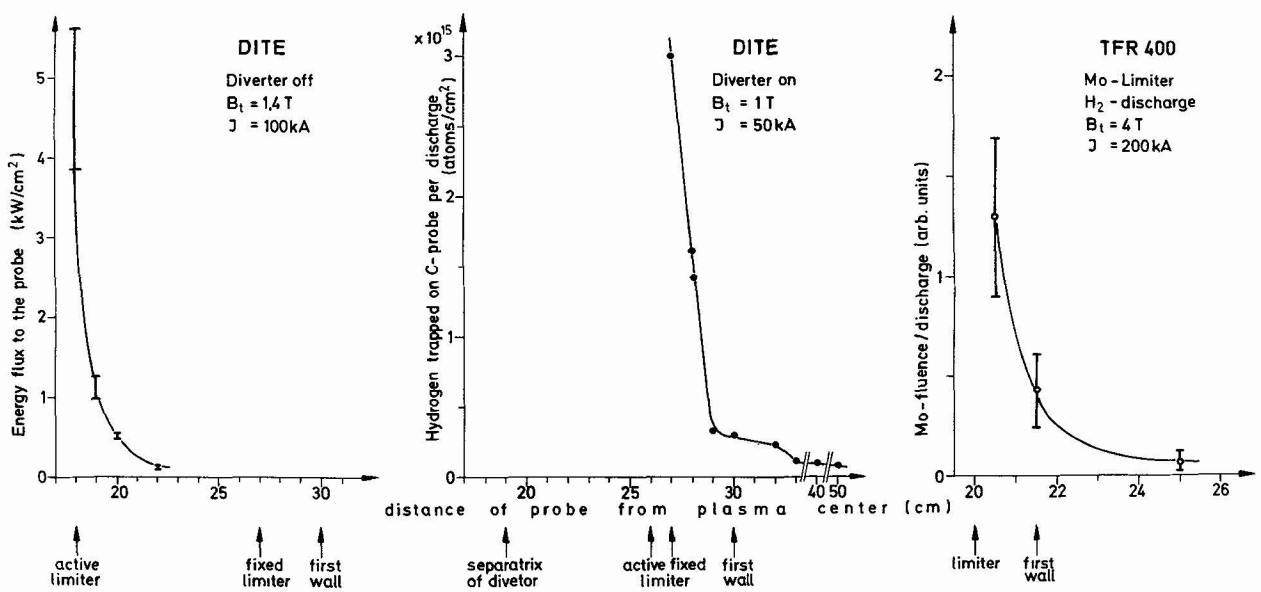

FIG. 2. — The energy flux, the hydrogen flux, and the impurity flux measured on a probe inserted into the space between the plasma boundary and the first wall at different positions.

3. **Interactions at the first wall and fluxes to the plasma.** — The first question is how do the hydrogen atoms come back into the plasma in order to keep the plasma density constant. This has not been investigated experimentally in detail up to now. In discharges with relatively clean walls the plasma density generally drops during the discharge [25-27]. This is mostly compensated by feeding in cold gas from the outside. By feeding in a surplus of gas it is also possible to increase the plasma density during the discharge.

From discharges where the filling gas has been changed from one hydrogen isotope to another the new isotope is replaced at the beginning of the discharge and predominantly the previous isotope is found in the plasma [28, 29, 30]. This shows that the walls had been implanted in the previous discharges with an amount of gas larger than the amount of gas in the discharge. Due to the exchange between the gas in the plasma and in the first wall this gas comes into the plasma.

The impurity concentration found in today's plasmas is much higher than the concentration in the initial filling gas. In order to obtain ignition, the concentration must be much lower than found today [31].

It is not clear which are the dominant processes causing the release of wall atoms, however, the following picture is generally assumed. At the begining of the discharge mostly oxygen and sometimes carbon enter the plasma by desorption of H_2O, CO, CO_2, oxygen or hydrocarbons (CH_4). The walls in today's plasma machines are not atomically clean. It has also been found recently that hydrocarbons are formed between the discharges by a reaction of the hydrogen atoms implanted at the end of a discharge with the carbon contained on the first wall [16].

During the discharge the oxygen and hydrogen hitting the first wall will cause desorption and sputtering of adsorbed layers, as well as metal of the wall material, thus reproducing and/or increasing the impurity concentration in the plasma.

In today's tokamak discharges it further been observed that the metal impurity concentration in the plasma increases when the oxygen concentration decreases, i.e. the more clean the first walls are getting [32, 33]. This phenomenon is not understood and may have several causes.

a) The plasma temperature near the wall, i.e. the mean energy of the particles bombarding the first wall may be slightly increased for the more clean discharges, but measured temperature distributions show that this is not sufficient to understand the effect [32].

b) The sputtering yields of oxides are generally lower than those for pure metals. However, for stainless steel (mostly Cr_2O_3) this effect is small, i.e. below a factor of 3 [34].

c) The particles released from the first wall by sputtering are generally mostly neutrals. However, at oxyde layers and contaminated surfaces the released wall atoms and molecules can be predominantly ions [35, 36]. These will be bent back to the first wall and may not enter the plasma. Thus the increased impurity concentration of metals in the plasma would mean that finally most of the released wall atoms are neutral and can now penetrate into the plasma. Thus the impurity problem may become more severe when the walls become cleaner.

4. **Atomic data needed for plasma surface interactions.** — In order to better understand and control the plasma wall interaction, and to be able to make predictions for larger machines the elementary processes at the first wall have to be known in some detail. The main processes of interest which have been reviewed recently [16] to [18] are :

1) Desorption of surface layers by ions, electrons and electromagnetic radiation.
2) Ion backscattering.
3) Ion trapping and reemission.
4) Sputtering (physical and chemical).
5) Surface changes due to prolonged ion bombardment.
6) Evaporation and disintegration due to overheating, which is nonuniform in space and time.

5. **Desorption.** — The surface of a solid is generally covered with several layers of foreign atoms and molecules which are chemically bound (O, C) or physically adsorbed (H_2O, CO, CO_2, CH_4, H_2). The desorption yields of these layers due to the impact of atoms, electrons and radiation must be known for understanding the impurity introduction during the plasma discharges and in order to optimise the cleaning procedures of the inner surfaces of today's plasma vessels. The data available deal mostly with electron and photon desorption from well prepared smooth surfaces [37] and only few investigations have been made for ion desorption [38, 39]. The desorption yields reported are generally in the range of 10^{-4} to 10^{-1} atoms per ion or electron [12, 37-39], but these may not necessarily apply for the contaminated surfaces of today's discharge chambers.

Oxygen and carbon which are well bound at a surface in the form of oxide or carbide additionally undergo chemical reactions with atomic hydrogen forming H_2O and CH_4 [16, 40]. These molecules are only weakly bound at the surface and can easily be desorbed in a discharge [16, 17]. This process, on the other hand, indicates the most promising way to remove effectively the oxide, carbon and carbide layers from the inner surfaces of the plasma chambers. During discharge cleaning, the plasma parameters and the first wall temperature have to be adjusted in order to maximise the H_2O and CH_4 production. This has been applied at Dite [19] and with some success at Alcator and Microtor [27, 42].

6. **Ion backscattering.** — Energetic light ions and neutrals impinging on a solid mostly penetrate the surface and are slowed down in collision with the electrons and atomic nuclei in the solid (Fig. 3). Depending on the type of ions and their energy, as well as the target material, some trajectories will be bent back, and thus part of the ions will leave the surface, i.e. become backscattered. Fast neutrals and ions will behave in the same way, as they all penetrate the solid as ions.

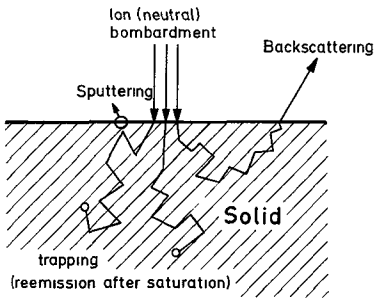

FIG. 3. — Trajectories of energetic ions impinging on a solid.

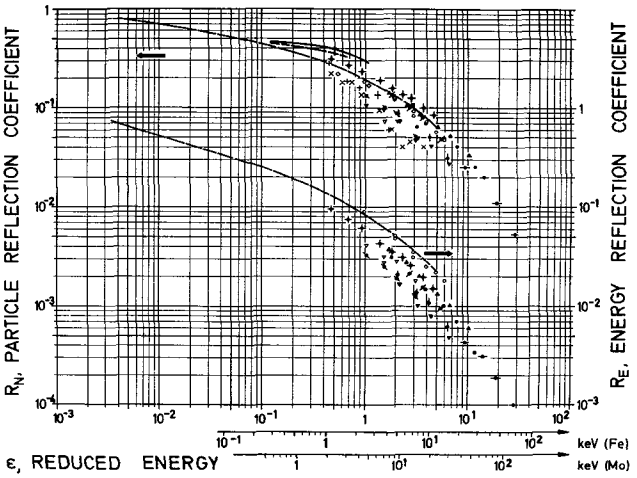

FIG. 4. — Particle and energy reflection coefficients as determined by different authors : OH → SS, □ D → SS, ▽H → Nb (annealed), ▽H → Nb (not ann.) ◇D → Nb (not ann.) (ref. [50]), OH → SS, ▼H → Nb, ▲H → Cu ⊸ H → Al, ⊸ H → Mo, ⊸H → Ag, ⊸H → Ta, ⊸H → Au (ref. [51]), + H → Zr, × H → Ti (ref. [52]), ——— ref. [43], – – – ref. [44, 45], ····· ref. [42].

Total backscattering yields and backscattered energy, as well as the energy- and angular distributions of the backscattered atoms, have been calculated analytically [43, 44] and by computer simulation programs which follow the individual ion trajectories [45] to [48]. Experimental determination of backscattering yields and distributions are difficult, as in the energy range of interest most of the backscattered particles are neutral. The most successful way of ionising the neutrals is a gas-filled stripping cell, as used also in neutral particle measurements in plasma experiments [49]. Such a cell could be calibrated to energies as low as 130 eV [50].

The results for total backscattering yields and backscattered energy of hydrogen ions on different materials are shown in figure 4, [43] to [46], [51] to [53]. The values are plotted as a function of a dimensionless universal energy given by [54].

$$\varepsilon = \frac{M_2}{M_1 + M_2} \frac{a}{Z_1 Z_2 e_0^2} E$$

where M_1, Z_1 and M_2, Z_2 are the masses and charge numbers of the incident ions and the target atoms, e_0 is the elementary charge ($e_0^2 = 14.39$ eV Å) ; a is the Thomas Fermi screening length given by :

$$a = 0.486(Z_1^{2/3} + Z_2^{2/3})^{-1/2}$$

and E is the incident energy in eV. In the two lower scales of figure 4 also absolute energies for stainless steel (Fe) and Mo are introduced. Especially for stainless steel the agreement between calculated and measured values is very good, which gives some confidence in the calculated values at low energies. where no measurements are available, but which are of special interest in fusion research.

The energy distribution of the backscattered atoms for normal incidence of hydrogen on stainless steel has only been measured for energies above 2 keV [50] while for 5 keV and 100 eV computed spectra for a copper target have been published [45] to [47]. For plasma simulation codes the energy range between 10 eV to 10 keV is of interest, but only histogramms with relatively broad energy ranges for the backscattered particles are needed. Such curves obtained by a smooth interpolation between the known spectra are plotted in figure 5, together with the exact spectra. The energy ranges are chosen according to those used in the Düchs code [15]. The intensities give absolute values, as backscattering coefficients are taken into account. For incident energies above 2 keV there is a maximum in the backscattered intensity at 1 to 1.5 keV, while at lower incident energies the maximum is close to the incident energy.

As mentioned already, most of the backscattered atoms are neutrals and only less than 5 % have a positive or negative charge [51].

The angular distribution of the backscattered atoms measured for 10 keV hydrogen atoms at normal incidence on Nb is nearly a cosine distribution [55]. For lower energies the calculations show also a cosine distribution [46], but no measured data are available.

7. **Ion trapping and reemission.** — Those ions and fast neutrals not directly backscattered come to rest in the solid. After slowing down they generally occupy interstitial positions and may diffuse further. Depending on the solubility, the diffusivity, and the barrier at the surface, they may either diffuse into the bulk of the solid, they may partly leave the surface, or they may be trapped in the implanted layer [56].

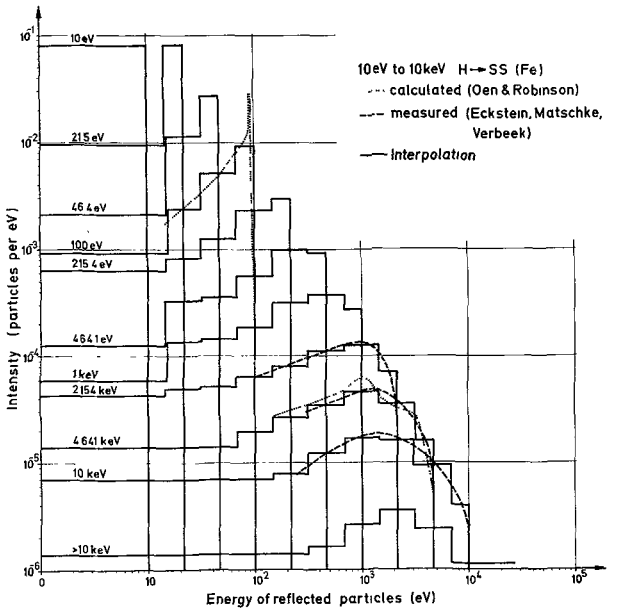

FIG. 5. — Energy distribution and intensity of hydrogen atoms backscattered from stainless steel. The incident energy is given on the left side above the curves. The measured values are determined at an angle of emergence of 45 deg [50] while in the calculated values all angles of emergence are included [45]. The histograms are a smooth interpolation between the measured and calculated values.

In the case of *high solubility*, as for hydrogen in titanium and zirconium, all ions coming to rest in the solid reside at interstitial sites, if the temperature is high enough for good diffusion, but low enough so that thermal desorption is negligible [16, 53, 56].

If the *solubility* of the incident *gas ions in the solids is low*, as for He bombardment of most metals and for hydrogen bombardment of several metals, for example stainless steel or molybdenum, the ions come to rest at interstitial positions in the solid, and they will diffuse until they become relatively stably trapped at damage sites, predominantly vacancies [57]. This is shown in figure 6 for ^{3}He implanted at different doses

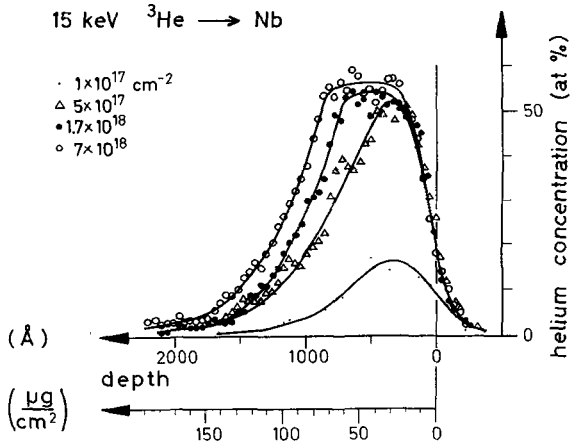

FIG. 6. — Implantation profiles of ^{3}He in Nb for different bombardment doses. At a dose of 5×10^{17}/cm^2 blistering had occured while at a dose of 7×10^{18}/cm^2 the spongy like surface structure has started to develop (ref. [58]).

into polycrystalline Nb [58]. The profiles have been obtained using the ^{3}He(d, p)^{4}He nuclear reaction. At the lowest dose the implantation profile mostly follows within the statistics of the measurements, the calculated distributions. At higher doses a saturation concentration of $\sim$ 50 atomic % is reached, after which the distribution tends to a rectangular profile within the range of the incident ions.

As the range of the ions increases with the incident energy, the total amount of trapped gas also increases with energy. The maximum concentration reached within the range of the ions is independent of the implanted energy, but decreases with the target temperature [59, 60]. The gas emitted after saturation is presumably released with an energy corresponding to the temperature of the first wall.

8. **Sputtering.** — Physical sputtering is the removal of surface atoms from a solid via a collision cascade initiated in the near surface region by incident energetic particles such as ions, neutrals, neutrons or electrons. Thus sputtering can be regarded as radiation damage in the surface. During the spread of the cascade the surface stays cold, contrary to surface removal by evaporation.

The sputtering yields, i.e. the number of atoms removed per incident particle, have been investigated for more than 100 years. However, the data available for the parameters of interest in fusion research are still poor, as has been shown in a recent review [17]. In figure 7 and in figure 8 the sputtering yields for

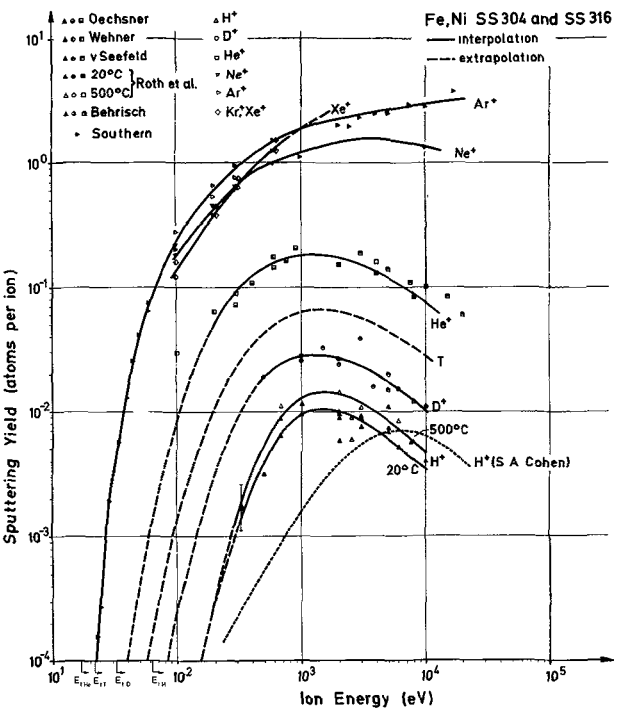

FIG. 7. — Sputtering yields for normal incidence of different ions on Fe, Ni, SS 304 and SS 316 as measured by different authors (ref. [17, 18], [61] to [69]). The values used in the plasma simulation of ref. [15] (S. A. Cohen) are also introduced.

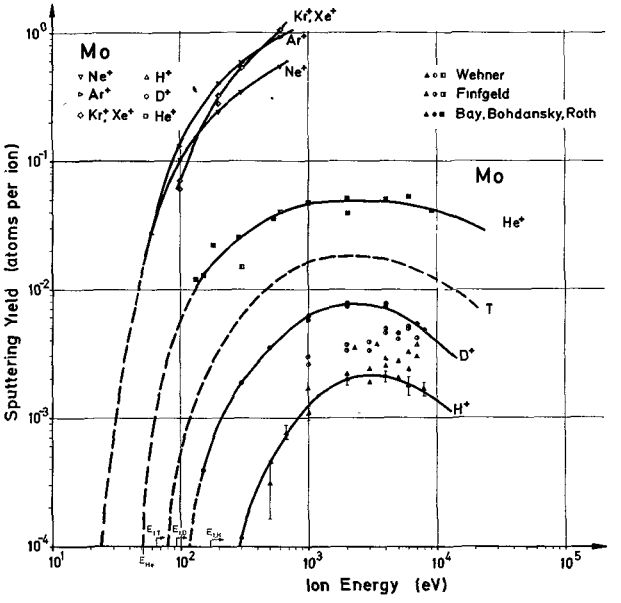

FIG. 8. — Sputtering yields for normal incidence of different ions on cast molybdenum as measured by different authors (ref. [64] to [67]). The solid lines are fitted to the experimental points, while the dashed lines are extrapolations.

normal incidence of different ions on stainless steel, nickel or iron and for cast molybdenum are summarized [17, 18]. They have been obtained with mass analysed ion beams partly by weight loss, partly by measuring the decrease of a thin film by Rutherford backscattering and partly by activation analysis of the target [61] to [69].

Below a threshold energy, E_t, of 20 to 200 eV no sputtering occurs. Yields then increase with energy to a maximum, which occurs for hydrogen at an energy around 2 keV. The decrease at a further increase of bombarding energy is due to the decrease of the deposited energy in the surface region. The difference between 20 °C and 500 °C for SS is due to different surface compositions at the different temperatures [65]. The dependence of the sputtering yield on the mass of the incident ion is much larger at low energies than at high energies. This could be expected, since the predicted threshold energy for sputtering by D is 1/2, and by ^{4}He is 1/4, of the threshold energy for proton sputtering. Thus at energies where the sputtering yield for protons is zero, the heavier ions, such as D, T and He, still show considerable sputtering.

Around a few 100 eV the sputtering yields of heavy noble gas ions, which would include also the yields for O and C, are about 10^3 times higher than the hydrogen sputtering yields. This means that a few percent O or C in the particle current hitting the first wall causes much more sputtering than the hydrogen.

The dependence of the sputtering yields on the angle of incidence has hardly been investigated. The few measurements have confirmed the theoretically expected increase of the yields with $(\cos\theta)^{-f}$ where $1 < f < 2$ and θ is the angle of incidence with respect to the normal [8]. This should hold for $\theta < 80°$; for larger θ the sputtering yields are expected to decrease to zero.

The atoms removed from clean surfaces are predominantly neutral, while from contaminated surfaces a large amount of atoms and molecules are emitted as ions [35, 36]. Their energy and angular distribution have not yet been measured for the parameters of interest. It is expected that the mean energy will be low (1 eV to 10 eV) and that the atoms will be emitted in a nearly cosine distribution [8, 17].

Results on neutron sputtering yields have achieved great attention due to extremely high yields of 0.3 atoms/neutron found in some experiments [71]. However, the latest, more careful investigation at several places have led to the conclusion that neutron sputtering yields are below 10^{-4} atoms/neutron, in agreement with theoretical predictions [6, 8, 72, 73].

If the bombarding ions can form a volatile compound with the target material, such as for hydrogen bombardment of carbon, an increased erosion yield due to the formation of CH_4 is expected. This has been found at target temperatures of 400° to 800 °C, as shown in figure 9 for different bombarding energies at

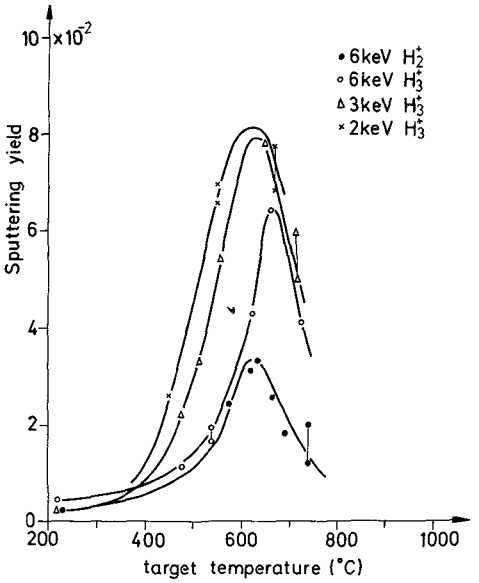

FIG. 9. — Temperature dependence of the sputtering yield of pyrolytic graphite for hydrogen bombardment at different energies (ref. [70]).

normal incidence [70]. The steep increase in the yields has been explained by increased mobility of H on the surface, so that CH_4 can be formed. The decrease of the yields at temperatures above 700 °C is not yet fully understood; it may be explained by an increased release of hydrogen from the surface, so that the probability for the formation of CH_4 decreases.

Similar effects have been found for silicon carbide and boron carbide. However, in these cases the surfaces seem to become depleted of carbon after some

dose, and chemical sputtering disappears, except when the target temperature is high enough so that carbon diffuses from the bulk into the depleted layer [17, 74].

Finally, in all compounds and alloys a composition change due to preferential sputtering by ion bombardment is expected and has partly been observed [17]. However, systematic investigations for the parameters of interest in respect to CTR have not yet been performed.

9. **Surface changes due to prolonged ion bombardment.** — If the incident gas ions are not soluble in the material, transmission electron microscope observations have shown that at bombarding doses of $\gtrsim 10^{16}/\text{cm}^2$, corresponding to several atomic percent gas injected into the solid, the gas starts to coalesce to small bubbles of 10 to 30 Å diameter inside the implanted layer [9, 75].

If the ion bombardment is increased further, blisters, i.e. bending up of a surface layer, can be observed [3, 4, 17, 75]. The critical dose for the appearance of blisters lies between 10^{17} and 10^{18} ions/cm^2. It depends on the bombarding energy, the current density and the angular and energy spread of the bombarding ions, as well as the material and its temperature [75] to [80].

If the bombardment is continued, several successive blister layers may be formed. At an ion dose corresponding to sputtering away a layer of about one deckeldicke, i.e. the thickness of the blister covers, blistering disappears and a spongy structure develops [10, 11, 17, 81], as seen in figure 10*a*, *b* for 5 keV H bombardment of stainless steel and in figure 11*a*, *b* for 100 keV He bombardment of niobium.

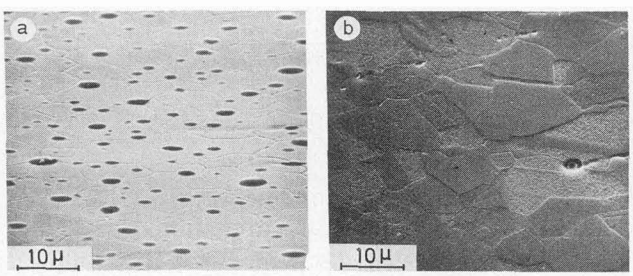

FIG. 10. — Surface topography of 304 stainless steel bombarded with different doses of 7.5 keV hydrogen ions at room temperature and normal incidence. Blistering is observed only at low bombarding doses (*a*). At higher doses (*b*) the surface becomes rough and the differently oriented grains are eroded at different rates (ref. [10] and [68]).

Further, blistering is considerably reduced if the bombardment is performed at a broad energy distribution and/or a broad angular distribution of the incident ions [80, 81] and the spongy structure occurs already at lower doses.

The temperature also can modify the blister appearance [3, 4, 58, 76] to [78], [82]. At medium temperatures (500 to 800 °C) blistering generally is increased and exfoliation of the blister covers is observed. At a further increase in temperature blistering is decreased again.

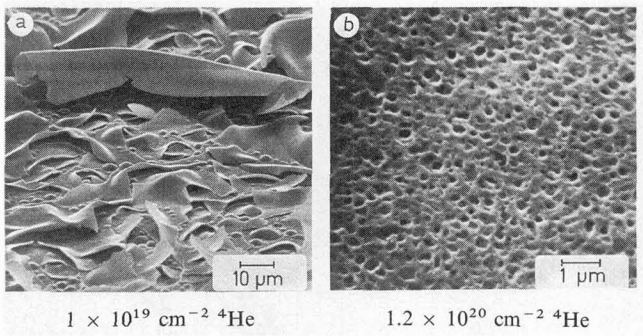

FIG. 11. — Surface topography of polycrystalline Nb at room temperature bombarded with different doses of 100 keV He ions at normal incidence. Blisters disappear after about one deckeldicke has been removed by sputtering (ref. [81]).

10. **Evaporation.** — The *steady state evaporation rate* $\dot{n}$ (atoms/cm^2 s) of atoms from a surface heated in equilibrium to a temperature T is given by

$$\dot{n}(T) = \alpha\, 3.5 \times 10^{20} \frac{p[\text{torr}]}{\sqrt{M.T[\text{K}]}} \left[\frac{\text{atoms}}{\text{cm}^2\ \text{s}}\right]$$

where p is the vapour pressure of the material, M its atomic number and α the sticking probability of atoms of the material with a temperature T at the surface. Generally, $\alpha < 1$, but for simplicity $\alpha = 1$ is taken. Vapour pressures and evaporation rates for different materials of interest are given in figure 12 [10, 83, 84]. If the impurity introduction in the plasma by evaporation from the limiter or the first wall should be smaller than by sputtering, we find for stainless steel a maximum temperature of about 850 °C, while for the refractory metals the maximum operation temperature ranges up to 2 000 °C. However, small contents of impurities, such as oxygen in the material, can largely increase the evaporation yields.

In a fusion reactor also *pulse evaporation* will occur as the energy deposition on the first wall may not be uniform in space and time. A local increased energy deposition will cause an increased surface temperature and thus increased evaporation. If an amount of energy E is coming to a first wall area A in the form of a heat pulse of duration τ, the increase in wall temperature ΔT will depend on the density ρ, the thermal conductivity k and specific heat c_p of the solid and is given by [8] :

$$\Delta T = \frac{E}{A} \frac{1}{\sqrt{\tau}} \sqrt{\frac{4}{\pi c_p . k \rho}}$$

As the temperature increases with the reciprocal square root of the deposition time, small values of τ, as may occur in a disruptive instability, can lead

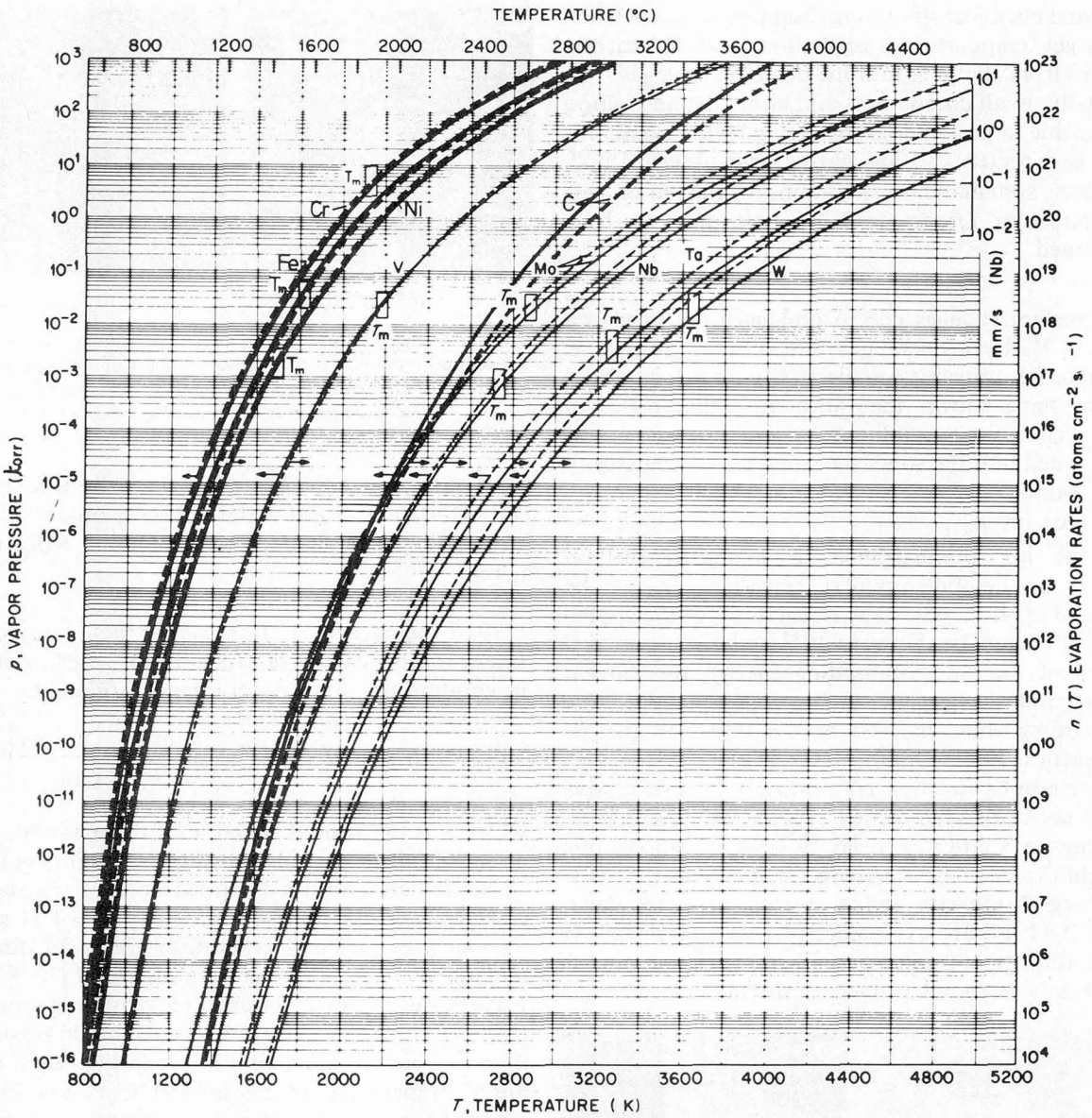

FIG. 12. — Vapour pressure and evaporation rates for different first wall materials calculated for $\alpha = 1$ (ref. [10], [83, 84]).

locally to extremely high wall temperatures [8]. These temperature pulses firstly cause a pulse evaporation, but may also very efficiently crack brittle materials [33, 85].

Pulse evaporation yields have been estimated for niobium [8] to be about

$$n \sim 0.2\, \tau \dot{n}(T_{\max}) .$$

The yields are generally small if $T_{\max} = T + \Delta T$ is not too high. No measured values seem to be available.

11. **Summary and conclusions for plasma experiments and later fusion reactors.** — In today's plasma experiments, especially of the tokamak type, the impurities introduced during the start of the discharge by desorption (as O, and C) dominate the achievable plasma parameters and also the further release of impurities from the first wall by sputtering.

Due to chemical reactions between the hydrogen and O or C at the wall i.e. the formation of H_2O and CH_4, clean hydrogen discharges may be obtained only if O and C are nearly quantitatively removed from the first wall. This may be achieved by glow discharge cleaning where H_2O and CH_4 production is maximised.

In order to reduce the impurity introduction into the plasma by sputtering, the wall bombardment has to take place at very low energies, this means at very low plasma temperatures near the first wall. For D, T discharges these have to be lower than for hydrogen discharges. This corresponds to a cold gas or a cold plasma blanket ; however, it is not yet clear whether this shift of the temperature gradient from the plasma wall transition into the plasma or gas near the wall can be achieved [86].

The reduction of the impurity concentration in the

plasma by introducing a divertor has to be studied, and much more quantitative information about plasma wall interaction processes has to be collected.

Acknowledgments. — It is a great pleasure to thank P. Ginot, G. M. McCracken and my colleagues, especially J. Bohdansky, D. F. Düchs, B. M. U. Scherzer, Ph. Staib, G. Staudenmaier and H. Vernickel for several discussions on the status of plasma wall interactions and the QWAASS measurements.

References

[1] HINNOV, E., *J. Nucl. Mat.* **53** (1974) 16.
[2] REBUT, P. H., DEI-CAS, R., GINOT, P., GIRARD, J. P., HUGET, M., LECOUSTAY, P., MORRIETTE, P., SLEDZIEWSKI, Z., TOCHON, J., TOROSSIAN, A., *J. Nucl. Mat.* **53** (1974).
[3] Proc. of the Int. Conf. Surf. Effects in Contr. Fusion Devices, Argonne, 1974, publ. in *J. Nucl. Mat.* **53** (1974).
[4] Proc. of the Int. Conf. Surf. Effects in Contr. Fusion Devices, San Francisco, 1976, to be published in *J. Nucl. Mat.* **63** (1976).
[5] Proc. of the Int. Symp. on Plasma Wall Interactions, Jülich, Oct. 1976, publ. as EURATOM report, Brussels, 1977.
[6] KAMINSKY, M., *IEEE Trans. Nucl. Sci. NS* **18** (1971) 208.
[7] VERNICKEL, H., *Nucl. Fusion* **12** (1972) 386.
[8] BEHRISCH, R., *Nucl. Fusion* **12** (1972) 691.
[9] MCCRACKEN, G. M., *Fusion Reactor design problems, Nucl. Fusion Special Supplement* (1974) 471.
[10] BEHRISCH, R., KADOMTSEV, B. B., *Plasma physics and control. Nucl. Fusion Research*, Proc. 5th Int. Conf. Tokyo, 1974, IAEA Vienna II (1975) 229.
[11] SCHERZER, B. M. U., *J. Vac. Sci. Technol.* **13** (1976) 420.
[12] COHEN, S. A., *J. Vac. Sci. Technol.* **13** (1976) 449.
[13] BADGER, B. *et al.*, University of Wisconsin Fusion React. Design, UWMAK I, UWFDM-68 (1973); UWMAK II, UWFDM-112 (1975); UWMAK III, UWFDM-150 (1976).
[14] MILLS, G. R. *et al.*, A fusion power plant. PPPL MATT-1050 (1974).
[15] MEADE, D. M., FURTH, H. P., RUTHERFORD, P. H., SEIDL, F. G. P., DÜCHS, D. F., *Plasmaphysics and Contr. Nucl. Fusion Research*, Proc. 5th Int. Conf. Tokyo 1974, IAEA Vienna I (1975) 621.
[16] MCCRACKEN, G. M. (ref. [5]).
[17] SCHERZER, B. M. U., BEHRISCH, R. and ROTH, J. (ref. [5]).
[18] BEHRISCH, R., Proc. of the *Summer School of Tokamak Reactors for Breakeven*, Erice, Sept. 1976, to be published EURATOM Report, Brussels 1977.
[19] STOTT, P. E., BURT, J., ERENTS, S. K., FIELDING, S. J., GOODALL, D. H. J., HOBBY, M., HUGILL, J., MCCRACKEN, G. M., PAUL, J. W. M., POSPIESZCZYK, A., PRENTICE, R., SUMMERS, D. R. (ref. [5]).
[20] STAIB, Ph., STAUDENMAIER, G. (ref. [5]) and private communications.
[21] ARTSIMOVICH, L. A., *Nucl. Fusion* **12** (1972) 215.
[22] WAGNER, F., MAYER, H. M. (ref. [5]).
[23] MEADE, D. M. (ref. [5]).
[24] STAIB, Ph. and STAUDENMAIER, G., *J. Nucl. Mat.* **63** (1976) 37.
[25] STOTT, P. E., DAUGHNEY, C. C., ELLIS, R. A., Jr., *Nucl. Fusion* **15** (1975) 413.
[26] MEISEL, D., KLÜBER, O., LAMIA, B., ENGELHARDT, W., FUßMANN, G., GERHARDT, J., GLOCK, E., KARGER, S., LISITANO, G., MCCORMICK, K., MAYER, H. M., MORANDI, P., SECNIC, S., WAGNER, F., *Plasmaphys. and Contr. Nucl. Fusion Research* Proc. 6th Int. Conf. Berchtesgaden 1976, IAEA Vienna (1977) and ref. [5].
[27] APGAR, E., COPPI, B., GONHALEKAR, A., HELAVA, H., KOMM, D., MARTIN, F., MONTGOMERY, B., PAPPAS, D., PARKER, R., OVERSKEI, D., *Plasmaphys. and Contr. Nucl. Fusion Research* Proc. 6th Int. Conf. Berchtesgaden 1976, IAEA Vienna (1977).
[28] ELLIS, R. B., PPPL, priv. Communication (1974).
[29] POSPIEZCYK, A., BURT, J., FIELDING, S. J., MCCRACKEN, G. M., STOTT, P. E. (ref. [5]).
[30] ENGELHARDT, W., KÖPPENDÖRFER, W., MÜNICH, M., SOMMER, J., 7th Europ. Conf. on Contr. Fusion and Plasmaphysics, Lausanne 1975, Vol. I (1975).
[31] MEADE, D. M., *Nucl. Fusion* **14** (1974) 289.
[32] MENSENVEY, E., BRETZ, N., DIMOK, D., HINNOV, E., PPPL MATT-1175 (1975) and *Nucl. Fusion* **15** (1975) 313.
[33] GINOT, P., TFR group, Fontenay-aux-Roses (ref. [5] and private comm.).
[34] BENNINGHOVEN, A. and MÜLLER, A., *Surf. Sci.* **39** (1973) 416.
[35] BENNINGHOVEN, A., *Surf. Sci.* **53** (1975) 596 and private communication.
[36] WITTMAACK, K., report GSF-P. 106, to be publ. in *Inelastic Ion Surface Collisions*, N. H. Tolk, J. C. Tully, W. Heiland, C. W. White eds (Acad. Press) 1977 and private communication.
[37] MENZEL, D., in *Interactions on Metal Surfaces*, R. Gomer (ed.), Topics in Applied Physics, Vol. 4 (Springer) 1975.
[38] MCCRACKEN, G. M., *Vacuum* **24** (1975) 463.
[39] TAGLAUER, E., BEITAT, U., MARIN, G., HEILAND, W., *J. Nucl. Mat.* **63** (1976) 193.
[40] BERGH, A. A., *The Bell systems technical Journal* XLIV (1965) 261.
[41] BLAUTH, E., MEYER, E., SCHWIRZKE, F., Proc. 5th Int. Conf. Ion. Phen. Gases, Munich, 1961 and *Z. Naturforsch.* **19** (1965) 549.
[42] TAYLOR, B., UCLA, private communication.
[43] WEIßMANN, R. and SIGMUND, P., *Rad. Eff.* **19** (1973) 7.
[44] BØTTIGER, J. and WINTERBON, K. B., *Rad. Eff.* **20** (1973) 65.
[45] ROBINSON, M. T., Proc. 3rd Nat. Conf. Atomic Coll. with Solids, Kiew 1954.
[46] OEN, O. S., ROBINSON, M. T., *Nucl. Instr. Meth.* **132** (1976) 647 and *J. Nucl. Mat.* **63** (1976) 210.
[47] ROBINSON, J. E. *et al.*, *Rad. Effects* **23** (1974) 29, *Appl. Phys. Lett.* **27** (1975) 425.
[48] ISHITANI, T., SHIMIZU, R., MURATA, K., *Japan J. Appl. Phys.* **11** (1975) 125 and to be published.
[49] BARNETT, C. F. and RAY, J. A., *Nucl. Fusion* **12** (1972) 65.
[50] MATSCHKE, F. E. P., ECKSTEIN, W., VERBEEK, H., *Verhdgl. DPG IV* **10** (1976) 47.
[51] ECKSTEIN, W., MATSCHKE, F. E. P., VERBEEK, H., *J. Nucl. Mat.* **63** (1976) 199.
[52] SIDENIUS, G., *Phys. Lett.* **49A** (1974) 409 and *Nucl. Instrum. Meth.* **132** (1976) 673.
[53] BOHDANSKY, J., ROTH, J., SINHA, M. K., OTTENBERGER, W., Proc. 9th Symp. Fus. Techn., Garmisch, June (1976).
[54] LINDHARD, J., SCHARFF, M., SCHIØTT, H., *Mat. Fys. Medd.* **33** No. 14 (1963).
[55] VERBEEK, H., *J. Appl. Phys.* **46** (1975) 2981.
[56] MCCRACKEN, G. M., *Rep. Progr. Phys.* **38** (1975) 241.
[57] KORNELSEN, E., *Rad. Eff.* **13** (1972) 227.
[58] BEHRISCH, R., BØTTIGER, J., ECKSTEIN, W., LITTMARK, U., ROTH, J. and SCHERZER, B. M. U., *Appl. Phys. Lett.* 27 (1975) 199.
[59] ROTH, J., PICRAUX, T., ECKSTEIN, W., BØTTIGER, J., BEHRISCH, R., *J. Nucl. Mat.* **63** (1976) 120.
[60] PISAREV, A. A. and TEL'KOVSKII, V. G., *At. Energ.* **38** (1975) 152.
[61] VON SEEFELD, H., SCHMIDL, H., BEHRISCH, R., SCHERZER, B. M. U., *J. Nucl. Mat.* **63** (1976) 215.
[62] BOHDANSKY, J., ROTH, J., SINHA, M. K., Proc. 9th Symp. Fusion Techn., Garmisch (1976).
[63] OECHSNER, H., Thesis, University of Würzburg (1963).

[64] ROSENBERG, J., WEHNER, U. G. K., *J. Appl. Phys.* **35** (1964) 1842.
[65] ROTH, J., BOHDANSKY, J., HOFER, W. O., KIRSCHNER, J., ref. [5].
[66] FINFGELD, C. R., Final report No. OKD-3557-15, Contract NO AT-(40-1), 3557, AEC Wash and Ruane Coll. Salem (1975).
[67] BAY, H., BOHDANSKY, J., ROTH, J., priv. Comm.
[68] BEHRISCH, R., BOHDANSKY, J., OETJEN, G. H., ROTH, J., SCHILLING, G., VERBEEK, H., *J. Nucl. Mater.* **60** (1976) 321.
[69] HOTSTON, E., *Nucl. Fusion* **15** (1975) 544.
[70] ROTH, J., BOHDANSKY, J., POSCHENRIEDER, W. and SINHA, M. K., *J. Nucl. Mat.* **63** (1976) 222.
[71] KAMINSKY, M. S., PEAVY, J., DAS, S., *Phys. Rev. Lett.* **32** (1974) 599.
[72] BEHRISCH, R., *Nucl. Instrum. Meth.* **132** (1976) 293.
[73] HARLING, O. K., THOMAS, M. T., Proc. 2nd topc. Conf. on the Techn. of Contr. Nucl. Fusion (Richland, Washington) Sept. 1976.
[74] BRAGANZA, C., MCCRACKEN, G. M., ERENTS, S. K., Proc. Symp. Phys. Ion Gases, Dubrovnik (1976) and *J. Nucl. Mat.* **63** (1976) 399.
[75] ROTH, J., *Appl. of Ion beams to materials*, Inst. of Phys. Conf. Series **28** (1975) 280.
[76] ERENTS, S. K., MCCRACKEN, G. M., *Rad. Eff.* **18** (1973) 191.
[77] KAMINSKY, M. S., DAS, S. K., *Rad. Eff.* **18** (1973) 245.
[78] BAUER, W., THOMAS, G. J., Proc. Int. Conf. on Defects and Defect Clusters in bcc Metals and their Alloys (1973) p. 255.
[79] ROTH, J., BEHRISCH, R., SCHERZER, B. M. U., *J. Nucl. Mater.* **53** (1974) 147.
[80] ROTH, J., BEHRISCH, R., SCHERZER, B. M. U., *J. Nucl. Mater.* **57** (1975) 365.
[81] BEHRISCH, R., SCHERZER, B. M. U., RISCH, M., ROTH, J., Proc. 9th Symp. Fusion Techn., Garmisch, June (1976).
[82] RISCH, H., SCHERZER, B. M. U., ROTH, J. (ref. [5]).
[83] HULTGREN, R., ORR, R. L., ANDERSEN, P. D., KELLEY, K. K., *Selected Values of Thermodynamic Properties of Metals and Alloys* (John Wiley) 1963.
[84] HONIG, R. E., KRAMER, D. A., *R.C.A. Review* **30** (1969) 285.
[85] SCHIVELL, J. F. and GROVE, D. J., *J. Nucl. Mater.* **53** (1974) 107.
[86] ENGELMANN, F., GOEDHEER, W. J., NOCENTINI, A., SCHÜLLER, F. C. (ref. [5]).